Systematic evaluation of amorphous silica production from rice husk ashes

José Arnaldo Santana Costa[*], Caio Marcio Paranhos

Polymer Laboratory, Department of Chemistry, Federal University of São Carlos, CEP 13565-905, São Carlos, São Paulo, Brazil

ABSTRACT

Amorphous silica (SiO_2) was extracted from the rice husk ashes (RHAs) of the agulhinha and cateto varieties. Optimized time, temperature, extractor concentration, and reaction time for a sustainable and cleaner production of SiO_2 from RHAs were studied. Textural and internal structures were analyzed by N_2 adsorption-desorption isotherms. The percentage of SiO_2 in the treated rice husks (RHs) increased by approximately 11 and 12% for the agulhinha and cateto varieties, respectively. The silica present in the RHAs remained predominantly amorphous for all of the times and temperatures investigated. The optimum parameters for calcination of the RHs were: 2 h at 700 °C. Type IV isotherms with type H1 hysteresis and good specific surface area values were observed. The optimum parameters for extraction of the amorphous silica were: concentration of $4 \, mol \, L^{-1}$ NaOH and 4 h of reaction. The extraction yield values were 80—99% and 83—97% for the agulhinha and cateto RHAs, respectively.

© 2018 Elsevier Ltd. All rights reserved.

1. Introduction

Industrial activities produce a certain amount of waste not related to the objectives of the production itself. Although a priority, the reduction of waste generation is technically limited; therefore, the best alternative is recycling (Della et al., 2005). With the increase in public awareness regarding sustainable development, the utilization of renewable resources is increasing. In the wake of problems associated with fossil fuels, biomass has been recognized as one the most important alternatives (Bazargan et al., 2015). However, one of the greatest difficulties for the proper disposal of biomass waste is the lack of processes and value-adding techniques that are compatible with its peculiarities (Della et al., 2005).

One of the most widely cultivated plants in the world is rice (Bazargan et al., 2015; Soares et al., 2015). In Brazil, as in many other countries, rice is one of the foods most consumed by the population, as well as being one of the main agricultural crops (FAO, 2015). The rice husk (RH) is the major by-product from rice milling, and on average it accounts for 20%, on a weight basis, of the paddy produced (An et al., 2010; Ng et al., 2015). The worldwide output of RH is around 1.2 billion tons annually, including 2.4 million tons in

Brazil. Because of the low levels of proteins and high ash content, most RHs in China are burned or buried. However, RHs are not easily decomposed by bacteria, due to their hard surface and high silicon and lignin content (Zhang et al., 2015). It is known that the incessant generation of solid waste materials represents a serious problem (Soares et al., 2015; Yeletsky et al., 2009).

The silica in RHs is amorphous and transforms into crystalline silica when it is heated at high temperatures — the transformation temperature is affected by its chemical purity and particle size (Othman Ali et al., 2011). Rice husk ash (RHA) derived from the unwashed husk contains about 96% (w/w) silica, as well as some organic compounds, alkali oxide, and impurities; however, with appropriate washing of the husk, the ash can contain >99% (w/w) silica (Muniandy et al., 2014). Thus, RHA can be used as an inexpensive alternative source of amorphous silica to produce silicon-based materials of technological interest (Zhang and Malhotra, 1996). However, analyzing several articles in the literature, it is possible to observe that none of them performs a systematic and chemometric study with the objective of optimizing the current variables for the extraction of amorphous silica from RHA, as well as the use of two different varieties of rice husks from Brazil (biogeographic differences).

The use of biomass as a dispersed source of energy for the conversion to energy and generation of RHA, from direct combustion, can contribute for a sustainable and cleaner production of nanostructured materials of technological interest. Since waste

---

recycling is a very important technique for attenuate the impacts caused to the environment. The RH and the RHA produced from it have attracted great interest in terms of the extraction of the SiO_2 component. Several studies have reported the different applications of silica extracted from RHs, Adam and Iqbal (2010) prepared heterogeneous catalysts for oxidation of styrene. Artkla et al. (2009) employed the photocatalytic degradation of tetramethylammonium in the hybrid catalyst of titania and MCM-41, while Bakar and Titiloye (2013) used catalytic pyrolysis for bio-oil production, and Wang et al. (2011) and Qiu et al. (2015) used commercial SiO_2 to prepare the Cu/SiO_2 catalyst. Previous studies have reported the use of silica for the synthesis of mesoporous adsorbent materials of the M41S family (e.g., MCM-41 and MCM-48) (Bhagiyalakshmi et al., 2010; Grisdanurak et al., 2003; Jang et al., 2009; Seliem et al., 2011; Wantala et al., 2012).

In this work, amorphous silica was extracted from the RHAs of the agulhinha (Indian origin) and cateto (Japanese origin) rice varieties. The parameters of calcination time and temperature for obtaining the RHAs were studied, and the extractor concentration and reaction time were evaluated for the extraction of amorphous silica from the RHAs obtained from the RHs.

2. Experimental

2.1. Collection and pretreatment of the RHs

Two different varieties of *Oryza sativa* rice were used for this work: agulhinha and cateto. The RHs were obtained from the Brazilian Agricultural Research Corporation (Embrapa), in São Carlos, São Paulo, Brazil.

The RHs were washed and rinsed separately three times with deionized water in order to remove unwanted materials. The RHs were then dried in an oven at 60 °C for 24 h, after which they were ground and sieved (48 mesh). Finally, 50 g of each variety of ground RH was placed under magnetic agitation in 500 mL of a solution of 3 mol L^{-1} HCl (Synth) at room temperature for 24 h, in order to remove impurities. Subsequently, the mixture was filtered under vacuum with deionized water until a constant pH was achieved, and then it was dried in an oven at 60 °C for 24 h.

2.2. Thermal treatment performed to obtain rice husk ashes (RHAs)

The thermal treatment was performed with the objective of optimizing the calcination time and temperature for obtaining the RHAs. The calcination was performed in a muffle furnace with a heating rate of 5 °C min^{-1}, in accordance with the experimental design shown in Table 1.

2.3. Acid treatment of the rice husk ashes (RHAs)

The acid treatment was performed only for the RHAs chosen from the experimental design (**item 2.2**). The A2-700 and C2-700 samples were chosen based on the analysis of the FTIR spectra and diffraction X-rays obtained, as well as the standard colors obtained after calcination of the RHAs. The RHAs were placed separately in a reflux condenser with a solution of 1 mol L^{-1} HCl, at the ratio of 5 g of RHA for each 50 mL of solution, for 2 h under magnetic stirring. After this period, the suspensions were filtered, and the solid residues were washed with deionized water until a constant pH was achieved, and they were then dried at 120 °C for 12 h.

2.4. Amorphous silica extraction

The amorphous silica was extracted from the RHAs in

Table 1
Experimental design for thermal treatment of rice husks in muffle furnace.

Time (h)	Temperature (°C)	Rice husk	
		Agulhinha	Cateto
		Sample identification	
1	500	A1-500	C1-500
2		A2-500	C2-500
4		A4-500	C4-500
1	600	A1-600	C1-600
2		A2-600	C2-600
4		A4-600	C4-600
1	700	A1-700	C1-700
2		A2-700	C2-700
4		A4-700	C4-700
1	800	A1-800	C1-800
2		A2-800	C2-800
4		A4-800	C4-800

accordance with the procedure described by Kalapathy et al. (2002), but with modifications. The extractions were taken from the RHAs of the two varieties studied, obtained in experimental design (A2-700 and C2-700 samples chosen in **item 2.3**). The amorphous silica was extracted by leaching with an extraction solution of sodium hydroxide (NaOH, Synth) at different concentrations under magnetic stirring at 80 °C and employing different times, in order to evaluate the most efficient extraction parameter from a second experimental design (Table 2).

The NaOH solution was added to the RHA in a polypropylene beaker, at a ratio of 10.0 mL of solution for each 1.0 g of RHA, under heating and intensive stirring. After the reaction period and cooling to room temperature (Reaction 1), the sodium silicate solution formed was filtered twice — first through quantitative filter paper with most pores 12 μm in diameter, followed by filtration through quantitative blue band filter paper with most pores 8 μm in diameter — and then stored in a sealed polypropylene flask at room temperature.

$$SiO_{2(s)} + 2\,NaOH_{(l)} \xrightarrow{\Delta} Na_2SiO_{3(l)} + H_2O_{(l)} \qquad \text{(Reaction 1)}$$
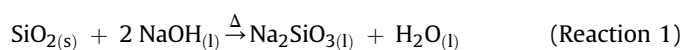
After filtration, the residue underwent successive washes with deionized water until a constant pH was reached, then it was dried at 110 °C for 24 h, and finally stored in a closed flask at room temperature. Diagram S1 shows the overall procedure.

2.5. Quantification of the amorphous silica content

The silica present in the sodium silicate solution was precipitated by treatment with a solution of sulfuric acid (H_2SO_4, Qhemis), and quantitated, by weighing on an analytical balance, as

Table 2
Experimental design for extraction of the amorphous silica.

NaOH (mol L^{-1})	Time (h)	Rice husk	
		Agulhinha	Cateto
		Sample identification	
1	1	A-1-1	C-1-1
	2	A-1-2	C-1-2
	4	A-1-4	C-1-4
4	1	A-4-1	C-4-1
	2	A-4-2	C-4-2
	4	A-4-4	C-4-4
8	1	A-8-1	C-8-1
	2	A-8-2	C-8-2
	4	A-8-4	C-8-4

amorphous silica, in accordance with reaction 2.

$$Na_2SiO_{3(l)} + H_2SO_{4(l)} \circledR SiO_2 + Na_2SO_{4\,(s)} + H_2O_{(l)}$$

(Reaction 2)
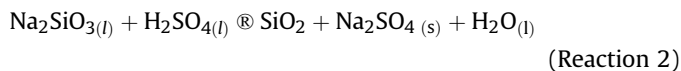
To a sodium silicate solution maintained at room temperature and under constant agitation in a magnetic stirrer, a solution of 5 mol L^{-1} of H$_2$SO$_4$ was added dropwise, in order to lower the pH of the solution to 9. The gels formed were kept at rest to react for 30 min, then they were crushed, dispersed in deionized water, and filtered under vacuum up to wash constant pH, then they were dried at 80 °C for 24 h and subsequently weighed, as summarized in Diagram S2. The results were submitted to analysis of variance (ANOVA), and the means of the replicates for each treatment performed were compared by the Tukey test at 5% probability, in order to determine the best extraction parameters for the silica.

2.6. Experimental design and statistical analysis

The factorial design used was chosen in order to determine the influence of two controllable quantitative variables: the concentration of the NaOH extraction solution, and the time taken in the extraction of silica from the RHA, as described in **items 2.4** and **2.5**. The SiO$_2$ yield obtained by precipitation is given by Equation (1):

$$\eta(\%) = \frac{m_{ext} \times 100}{m_{SiO_2}},$$

(1)

in which η (%) is the yield of amorphous silica (SiO$_2$), m$_{ext}$ (g) is the mass of amorphous SiO$_2$ obtained, and m$_{SiO2}$ (g) is the weight of the RHA used in the extraction.

ANOVA was used for the yield means of the repetitions of mass SiO$_2$ precipitation, which varied due to the reaction conditions: extractor solution concentration and reaction time. The means were compared via the Tukey test at 5% probability, using beta version 7.7 of the ASSISTAT software (Silva and Azevedo, 2002).

2.7. Characterizations of the rice husks (RHs) and the rice husk ashes (RHAs)

The RHs and RHAs were characterized by Fourier transform infrared spectroscopy (FTIR), X-ray fluorescence (XRF), thermogravimetric analysis (TGA), X-ray diffractometry (XRD), digital photographic images, and nitrogen adsorption-desorption isotherms — FTIR spectra and X-ray diffractograms were produced for the commercial silica (99.8% purity) to enable direct comparison with the RHAs obtained.

The FTIR spectra were obtained in the 4000–400 cm^{-1} region, using a Varian 3100 spectrophotometer, operated at room temperature, with a resolution of 4 cm^{-1} and number of scans equal to 32. The samples were prepared in the form of KBr pastilles. The chemical analyses were performed by X-ray fluorescence, using a Shimadzu EDX-720 spectrometer under the following conditions: vacuum atmosphere, 10 mm collimator, working range of 15–50 kV between atoms, and total analysis time of 100 s.

Thermogravimetric analyses were performed under a 20 mL min^{-1} flow of nitrogen, using a NETZSCH TG 209 F3 apparatus. Portions of the samples (~5.0 mg) were placed in alumina crucibles, and the temperature was increased from 35 to 900 °C at a rate of 20 °C min^{-1}. The samples were analyzed at room temperature, using a Shimadzu LabX XRD–6000 diffractometer operating with Cu Kα ($\lambda = 1.5406$ Å), in the 2θ range of 5–80°, in step scan mode with a width of 0.02°, a step time of 0.6 s, and a scanning rate of 2° min^{-1}.

In order to characterize the crystallinity of the different samples,

the crystallinity index (CrI) was determined based on the reflected intensity data, in accordance with the method of Johar et al. (2012):

$$\mathbf{CrI}\ (\%) = \frac{I_{002} - I_{am}}{I_{002}} \times 100,$$

(2)

in which $I_{0\,0\,2}$ is the maximum intensity of the (0 0 2) lattice diffraction peak, and I_{am} is the intensity scattered by the amorphous part of the sample. The diffraction peak for plane (0 0 2) is located at a diffraction angle of about $2\theta = 22°$, and the intensity scattered by the amorphous part is measured as the lowest intensity at a diffraction angle of about $2\theta = 18°$.

Photographic images of the RHAs were taken using a Canon G12 camera with a 4.5 aperture, speed of 1/100 s, ISO 800, and white correction for fluorescent light. Nitrogen adsorption-desorption isotherms were measured at −196.15 °C, using a NOVA 1200 volumetric adsorption analyzer. Prior to the analysis, approximately 100 mg of sample was evacuated at 300 °C for 1 h in the degas port of the instrument. The Brunauer-Emmett-Teller (BET) specific surface area was calculated using adsorption data in the relative pressure range of 0.01–0.95. The pore volume of the sample was determined from the amount of nitrogen adsorbed at a relative pressure of about 0.95, and pore size distribution curves were calculated from analysis of the adsorption branch of the isotherm, using the Barrett-Joyner-Halenda (BJH) algorithm.

3. Results and discussion

3.1. Characterization of the rice husks (RHs) and the rice husk ashes (RHAs)

3.1.1. Fourier transform infrared spectroscopy (FTIR)

The spectra obtained for the untreated agulhinha and cateto RHs, and the RHs treated with hydrochloric acid, are shown in Fig. 1. The broad absorption band near 3420 cm^{-1} was observed in all spectra, and it is representative of the C—H and O—H groups, which indicate water absorption. This band is attributed to the stretching of the hydrogen bonds and the bending of the hydroxyl (OH) groups that are bound to the cellulose structure present in the RHs (Johar et al., 2012; Yeh et al., 2015). These results indicate that the cellulose component was not removed from the RH during the acid
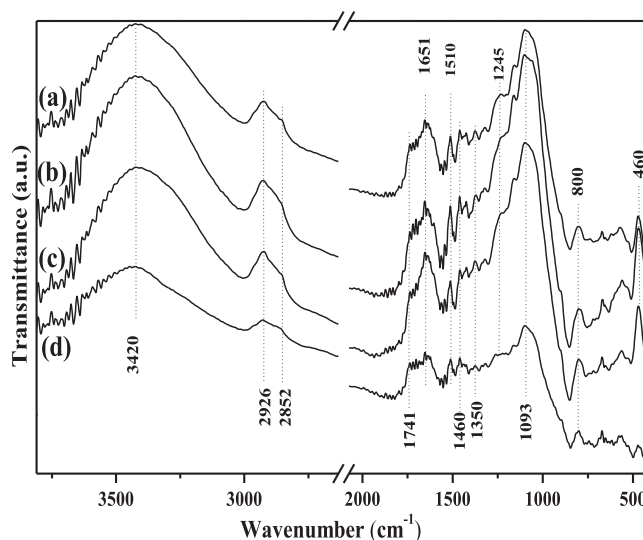

Fig. 1. FTIR spectra of rice husks: (a) untreated agulhinha, (b) agulhinha treated with hydrochloric acid, (c) untreated cateto, and (d) cateto treated with hydrochloric acid.

treatment conducted on the RH fibers (Johar et al., 2012). A similar trend occurred with another absorption band around 1651 cm^{-1}, which belongs to the O–H groups of the adsorbed water molecules (Das et al., 2014; Johar et al., 2012).

The band around 2926 cm^{-1} and a shoulder near 2852 cm^{-1} are attributed to the stretching and/or vibration of C–H due to the aliphatic-saturated compounds present in the cellulose and hemicellulose (Tran et al., 2014). A shoulder was observed around 1741 cm^{-1} in the spectra of the RHs, which is attributed to the acetyl and ester groups of the C=O bond in hemicellulose or carboxylic acid groups in the ferulic and *p*-coumaric components of the lignin (Das et al., 2014; Johar et al., 2012). This shoulder may be related to the wax or natural fat present in RHs (Tran et al., 2014).

The most characteristic infrared bands of lignin, which are found near 1510 cm^{-1}, represent the C=C aromatic skeletal vibrations. The bands in the range of 1426–1460 cm^{-1} are attributed to C–H deformation (asymmetric) and vibration of the aromatic skeleton, while the bands near 1350–1375 cm^{-1} are attributed to the symmetric and asymmetric deformation of either the C–H bond in methyl alcohol and phenols or the C–H balance in alkanes (Bledzki et al., 2010; Tran et al., 2014). The band around 1245 cm^{-1} is described as a C–O deformation in secondary alcohol and aliphatic ether. The large band around 1093 cm^{-1} is attributed to the asymmetric and symmetric stretching of bands of the Si–O–C and Si–O–Si bonds corresponding to the silica and the cellulose present in the RHs used. Finally, the bands present at 800 and 460 cm^{-1} are attributed to the stretching vibration of the Si–C and Si–O bonds, respectively (Costa et al., 2015, 2014; Santos et al., 2013).

Fig. 2a–2c illustrate the FTIR spectra of the agulhinha RHAs obtained from calcination of the agulhinha RH using different calcination times and temperatures. Fig. 2a shows a broad band around 3446 cm^{-1}, which is attributed to the stretching vibration of the O–H bond in Si–OH, and the HO–H vibration of the water molecules adsorbed on the silica surface (Carmona et al., 2013; Costa et al., 2017a). The narrow band around 1633 cm^{-1} is attributed to the bending vibration of the H$_2$O trapped within the silica matrix (Adam and Kueh, 2014).

The band around 1093 cm^{-1} is attributed to the asymmetrical stretching vibration of the Si–O–Si bond of the structural siloxane groups (Costa et al., 2014). The band around 807 cm^{-1} is attributed to the symmetric stretching vibration of the Si–O bond, while the band at 465 cm^{-1} is attributed to the vibration and bending modes of the Si–O–Si bond (Costa et al., 2017b, 2014).

The FTIR spectra of Fig. 2a indicated a narrow correlation between bands; however, it is possible to observe an increase in the intensity of the bands at 1093, 807, and 465 cm^{-1} with an increase in the calcination temperature of the RHs. This effect may be related to traces of organic matter from the cellulose in the RHAs obtained, mainly in the A1-500 and A1-600 experimental designs.

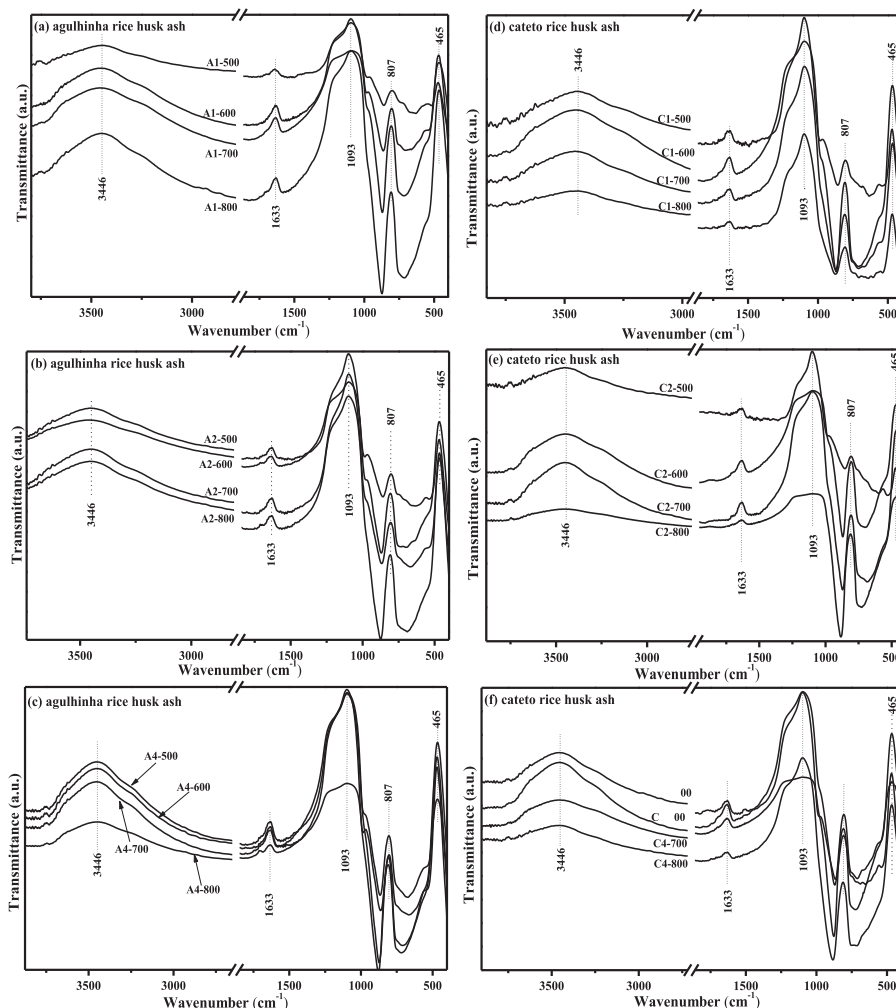Fig. 2b and c shows the RHAs obtained after 2 and 4 h of

Fig. 2. FTIR spectra of rice husk ashes (RHAs), obtained for different times and calcination temperatures: agulhinha RHAs for (a), (b), and (c); and cateto RHAs for (d), (e), and (f).
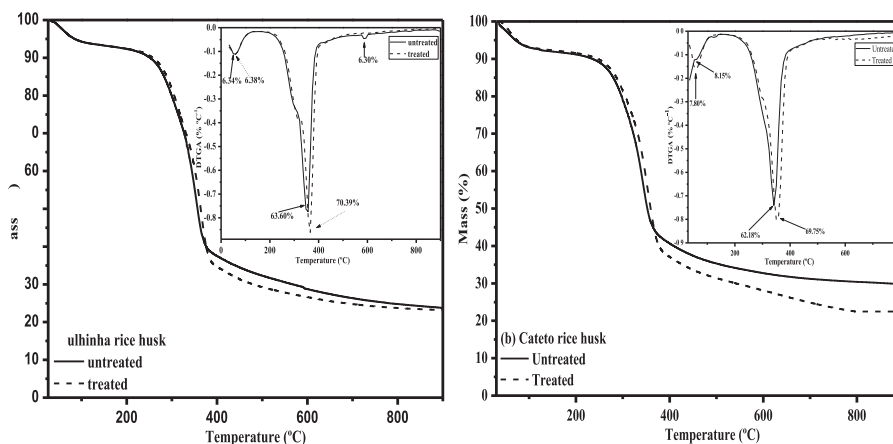
calcination, respectively, for the same temperatures that were studied in all of the graphs of Fig. 2. The RHAs obtained after 2 h (Fig. 2b) had the same behavior as the RHAs obtained after 1 h of calcination, which showed an increase in intensity in the 1093, 807, and 465 cm^{-1} bands with an increase in calcination temperature from 500 to 800 °C. For the spectra of the RHAs obtained at 4 h (Fig. 2c), it can be seen that there is practically no difference in the intensities of the bands obtained at temperatures of 500, 600, and 700 °C; however, it is possible to observe a decrease in intensity and a broadening of the band at 1093 cm^{-1} in the spectrum obtained at 800 °C (A4-800).

Fig. 2d–2f show the FTIR spectra for the RHAs obtained from calcination of the cateto RH using different calcination times and temperatures. Fig. 2d–2f show the same characteristic bands of silica that were observed for the agulhinha RHAs, with the same wavenumber intervals (3446, 1633, 1093, 807, and 465 cm^{-1}).

In the spectra of Fig. 2d, it is possible to observe a small band broadening at 1093 cm^{-1}, and an increase in intensity of the bands at 807 and 465 cm^{-1} when comparing the C1-600 and C1-700 samples with the C1-500 sample. It is also possible to see a decrease in the intensity of the 1093, 807 and 465 cm^{-1} bands in design C1-800 compared to earlier designs. In Fig. 2e, however, different behavior is observed — there is an increase in the intensity of the bands located at 807 and 465 cm^{-1} as the calcination temperature increases. There was only a small broadening of the band at 1093 cm^{-1} in the C2-600 and C2-800 samples compared to C2-500, and a loss of intensity was observed in this band in the C2-800 sample.

Finally, in Fig. 2f, it is possible to observe a small increase in the intensity of the 1093, 807, and 465 cm^{-1} bands in the C4-600 and C4-800 samples when compared to the C4-500 sample; however, no significant differences were observed in the spectra of the C4-600 and C4-800 samples. When compared with the other designs, in the spectrum of the C4-700 sample a decrease in intensity was observed, followed by a broadening of the band at 1093 cm^{-1}, while for the bands at 807 and 465 cm^{-1} there was a small increase in the intensity.

Fig. S1 shows the FTIR spectrum obtained from commercial silica with 99.8% purity. When compared to the spectra of the agulhinha and cateto RHAs, it can be seen that the spectra are wavenumbers corresponding throughout the spectral range analyzed, which further confirms the presence of silica in the RHs.

3.1.2. X-ray fluorescence (XRF)

Table 3 shows the chemical compositions for the untreated agulhinha and cateto RHs, and the RHs treated with HCl, as well as

the RHAs obtained from treated RHs calcined at 700 °C for 2 h. Compared to the untreated RHs, there was an increase of approximately 11.10 and 12.66% in the percentage of SiO_2 in the treated agulhinha and cateto RHs, respectively. However, the agulhinha variety has a higher percentage of SiO_2 when compared to the cateto variety. Also, in the agulhinha and cateto varieties, it can also be seen that the chemical composition of all the other oxides — which can be considered to be impurities (Real et al., 1996) — decreased with the acid treatment performed on the RHs, except for Na_2O (for both varieties) and Al_2O_3 (for the agulhinha variety only).

The results obtained for the RHAs show that the SiO_2 content increased by about 1.70 and 1.89% for the agulhinha and cateto varieties, respectively, in comparison with the treated RHs, indicating that the percentage of impurities decreased significantly with thermal treatment and subsequent acid treatment performed on the RHAs. The results also showed that the metal oxides or impurities that are most common in the RHs and RHAs are the ones formed by sodium, potassium, calcium, magnesium, copper, aluminum, iron, manganese, and zinc. However, the chemical composition may change, depending on the soil in which the rice is planted, the type and amount of fertilizer used, and the type of rice planted. The K_2O and P_2O_5 oxides present in the RHs and RHAs are generally derived from the fertilizers used in the rice crops, while other oxides — especially CaO, MgO, and Na_2O — come from the soil reservoir (Della et al., 2005, 2001).

Pretreatment of the RHs and RHAs with HCl after calcination was efficient for the removal of impurities, and also contributed to the production of a white RHA. The levels of SiO_2 found were higher than some of the values reported in the literature. The values found by An et al. (2010), Rambo et al. (2011), Della et al. (2002), and Chauhan and Kumar (2013) were 78.44, 91.40, 94.95, and 84.10% of SiO_2, respectively.

3.1.3. Thermogravimetric analysis (TGA)

Fig. 3 shows the TGA/DTGA curves obtained for untreated and treated RHs. It can be seen that the agulhinha RHs (Fig. 3a) had a mass loss event in the temperature range of 32–133 °C, which could be attributed to the elimination of adsorbed water, and the residual solvents physically adsorbed in the natural fibers of the RH. This is due to the hydrophilic nature of the natural fiber in the RH (Johar et al., 2012; Raabe et al., 2014). Another thermal event was observed in the temperature range of 180–453 °C, which could be attributed to the decomposition of the natural fibers present. According to Gu et al. (2013) and Carmona et al. (2013), hemicellulose, cellulose, and lignin begin to decompose at 200–260, 240–360,

Table 3
Chemical composition of the rice husks and rice husk ashes, after 2 h of calcination at 700 °C.

		Rice husk				Rice husk ash	
		Agulhinha		Cateto		Agulhinha	Cateto
		Untreated	Treated	Untreated	Treated	A2-700	C2-700
A	SiO_2	85.53	96.63	83.69	96.35	98.34	98.24
	Na_2O	1.47	1.95	0.26	2.26	0.32	0.14
N	MgO	0.13	0.11	0.06	0.00	0.02	0.03
A	Al_2O_3	0.59	0.64	0.54	0.47	1.15	1.31
	P_2O_5	1.60	0.26	1.08	0.50	0.05	0.11
L	K_2O	6.82	0.03	9.99	0.13	0.00	0.02
Y	CaO	2.02	0.04	2.78	0.02	0.02	0.01
	Cr_2O_3	0.13	0.02	0.14	0.03	0.02	0.02
T	MnO	0.64	0.03	0.42	0.04	0.02	0.02
E	Fe_2O_3	0.95	0.19	0.90	0.10	0.05	0.07
	CuO	0.09	0.06	0.07	0.06	0.02	0.02
(%)	As_2O_3	0.05	0.04	0.07	0.06	0.01	0.01
	CO_2	0.00	0.00	0.00	0.00	0.00	0.00

Fig. 3. TGA/DTGA curves of untreated and treated rice husks: (a) agulhinha and (b) cateto.

and 280–360 °C, respectively. It was not possible to separate the degradation processes of the RH components due to the complexity of the reactions and the superposition of the degradation events in the TGA/DTGA curves (Carmona et al., 2013; Raabe et al., 2014). Finally, the last event observed (for the untreated RH only), at 567–711 °C, could be attributed to oxidation of the residual organic matter (Raabe et al., 2014).

Fig. 3b shows the TGA/DTGA curves obtained for both untreated cateto RHs and those after acid treatment was performed, which resulted in two mass loss events. Similar to what was noted for the agulhinha variety, the first event is located in the temperature range of 35–158 °C, while the second event is located in the 158–496 °C range, and they are attributed to: the elimination of adsorbed water and residual solvents physically adsorbed in the fibers; and the decomposition of natural fibers present in the RHs, respectively (Carmona et al., 2013).

There was a small increase in the thermal stability of the RHs treated with acid, as evidenced by the shift in the TGA/DTGA curves for the treated RHs, especially in the second decomposition event. This was due to the removal of metal impurities by the acid treatment, as discussed in the XRF results. According to Della et al. (2001), some of these impurities form the glass phase and may lower the melting point of the RH. The amount of residues obtained from the treated RHs was lower — the residue percentages were 23.76 and 23.23% for the agulhinha variety, and 29.67 and 22.45% for the cateto variety, for the untreated and treated RHs, respectively.

3.1.4. X-ray diffractometry (XRD)

The XRD profiles obtained for untreated agulhinha and cateto RHs, and RHs treated with hydrochloric acid are shown in Fig. 4. The XRD profiles obtained have three well-defined crystalline peaks, around $2\theta = 16$, 22, and 35°, which are profiles typical of cellulose I, not hemicellulose and lignin, which are amorphous in nature (Johar et al., 2012; Klemm et al., 2005). According to Johar et al. (2012), cellulose has a crystalline structure due to hydrogen bonding interactions and van der Waals forces between adjacent molecules, and the acid treatment performed on natural fibers has no effect on the crystalline domains, but may dilute or destroy the amorphous region of the fiber. For the treated agulhinha and cateto RHs, it can be seen that the peaks around $2\theta = 22°$ showed a small increase in intensity compared to the respective untreated RHs. The presence of silica in the treated and untreated RHs was confirmed by the appearance of an intense peak around $2\theta = 22°$, which confirmed the results obtained in the FTIR spectra.
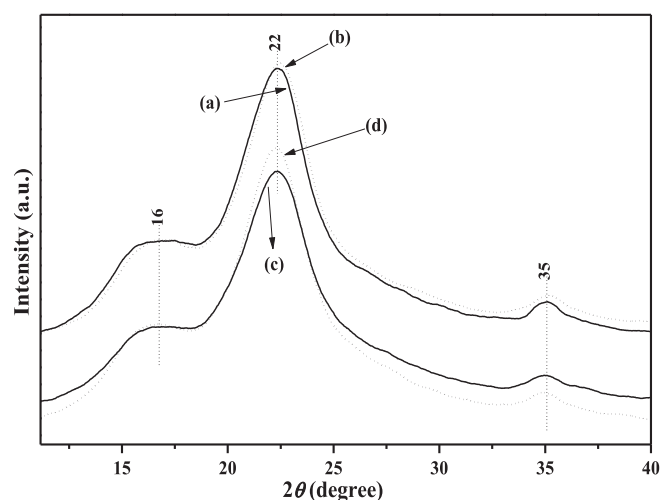
Fig. 4. XRD profiles of rice husks (RHs): (a) untreated agulhinha RHs, (b) agulhinha RHs treated with hydrochloric acid, (c) untreated cateto RHs, and (d) cateto RHs treated with hydrochloric acid.

The crystallinity index (CrI) values determined for the RHs are summarized in Table 4. An increase can be seen in the CrI value of the treated RHs — the same behavior was observed for both varieties of RH, which is due to the removal of amorphous non-cellulosic materials after acid treatment.

The XRD profiles obtained for the RHAs are for different calcination temperatures and times — see Fig. 5. The obtainment of amorphous and/or crystalline silica may be directly related to temperature, time, and the extraction method.

Fig. 5a and b shows that all of the RHA samples exhibit a single peak around $2\theta = 22°$, which is indicative of the presence of amorphous silica (Athinarayanan et al., 2015; Soltani et al., 2014). Thus, the silica present in the RHAs remained predominantly amorphous for all of the calcination times and temperatures tested.

The calcination temperature and time are important factors that define the amorphous and/or crystalline silica content in RHAs — a long time and a high calcination temperature cause the crystallization of the amorphous silica, due to the presence of potassium and sodium in the ash, which accelerates melting of the particles and crystallization of the cristobalite (Della et al., 2005). However, this phenomenon was not observed in this study because the maximum temperature applied was 800 °C — according to some

Table 4
Crystallinity index (CrI) for the rice husks.

Sample		CrI (%)
Agulhinha rice husk	Untreated	59.8
	Treated	64.9
Cateto rice husk	Untreated	60.3
	Treated	60.8

researchers (Chauhan and Kumar, 2013; Della et al., 2002; Ghorbani et al., 2013; Soltani et al., 2014), the crystallization of silica occurs at temperatures above 800 °C.

Fig. S2 shows the diffraction X-ray obtained for the commercial silica with 99.8% purity. When comparing the XRD pattern of the commercial silica with that obtained in the RHAs, a narrow correlation could be seen in the peak characteristic of the amorphous silica, which further confirms the presence of amorphous silica in the RHAs.

3.1.5. Digital photographic images

Table 5 shows digital photographic images of the RHAs obtained by calcination of the RHs at different times and temperatures. The A1-500 and C1-500 samples had the characteristics of a coarse black powder with a small number of ash particles from incomplete combustion of the organic matter. Samples A2-500, A4-500, C2-500, and C4-500 had the characteristics of a coarse brown powder, with a small number of ash particles, which was also from incomplete combustion. Sample C1-700 had the characteristics of a fine pinkish whitish powder, with a small number of ash particles. Additionally, other samples also had the characteristics of a fine pinkish whitish powder.

During the calcination process, it was observed that in order to obtain a high quality RHA, it is necessary to perform a homogeneous distribution of the RHs in the crucible, and it is essential to ensure air circulation inside the muffle oven in order to supply sufficient oxygen for complete combustion of the organic matter. Thus, when a larger volume of RHs is used for calcination, a black ash with a non-uniform texture may be obtained, due to the presence of residual carbon (Lee et al., 2013).

The FTIR, XRF, and XRD results, as well as the photographic images obtained for the RHAs, showed an ash with the characteristics of a fine white powder. Samples A2-700 and C2-700 were chosen as the basis for the designs for extracting silica gel from the ashes. From previous results, it is important to note that 700 °C was defined as the critical temperature in the process, based on two considerations: a) temperatures below 700 °C contribute to the presence of residual carbon; and b) temperatures above 700 °C contribute to the formation of non-reactive crystalline silica.

3.1.6. Nitrogen adsorption-desorption isotherms

The N_2 adsorption-desorption isotherms for the RHAs derived from agulhinha (A2-700) and cateto (C2-700) RHs, via calcination
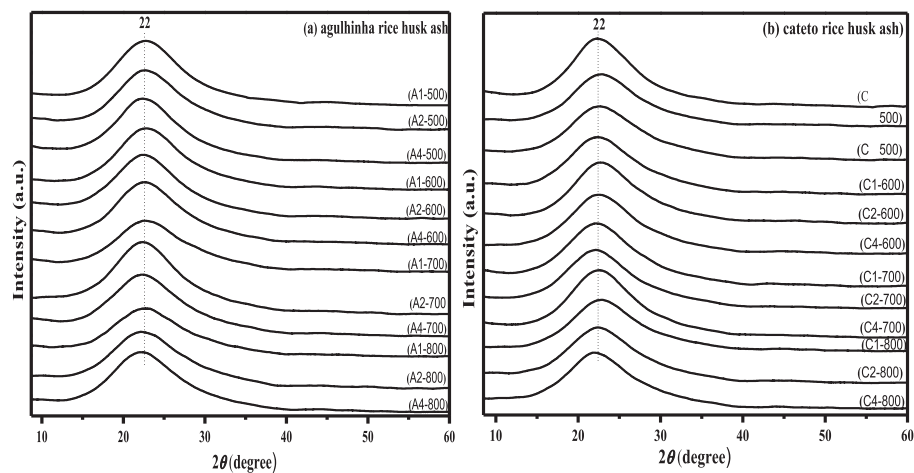
Fig. 5. XRD profiles of rice husk ashes (RHAs), obtained using different calcination times and temperatures: (a) agulhinha RHAs and (b) cateto RHAs.

Table 5
Digital photographic images of the rice husk ashes obtained with different calcination times and temperatures.
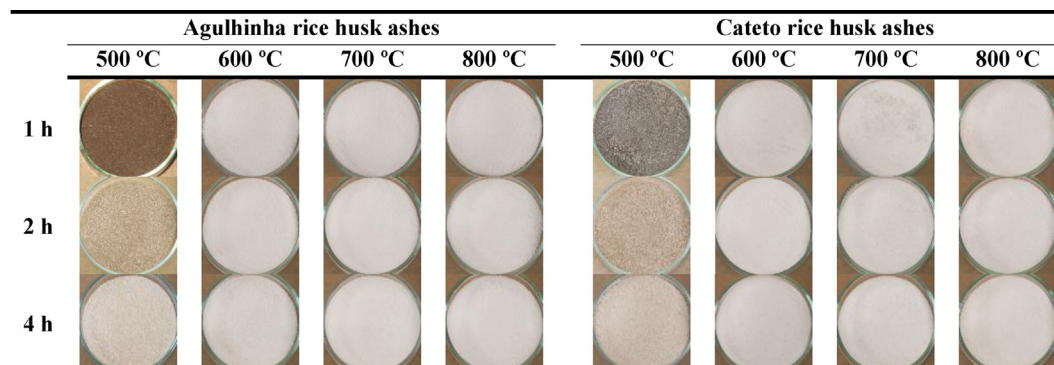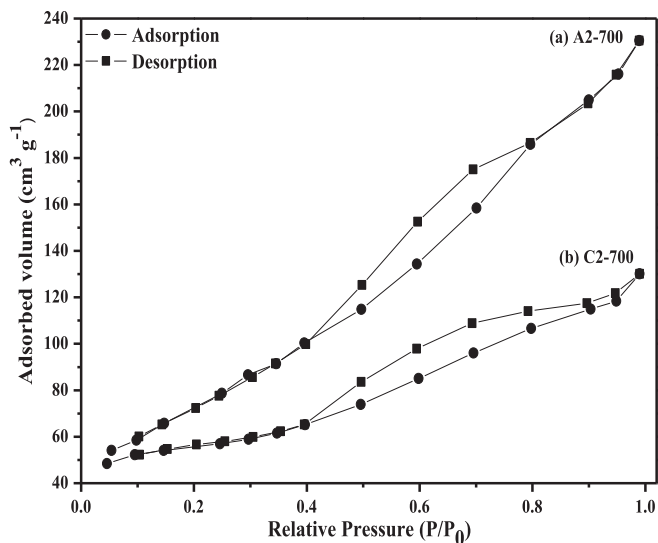
Fig. 6. Nitrogen adsorption/desorption isotherms of rice husk ashes (RHAs) obtained with 2 h of calcination at 700 °C: (a) agulhinha RHAs and (b) cateto RHAs.

at 700 °C for 2 h, are shown in Fig. 6a and b, respectively. The RHAs displayed type IV isotherms with type H1 hysteresis loops, according to the IUPAC classification (Costa et al., 2014). The existence of a hysteresis loop, which is associated with capillary condensation at relative pressures $(P/P_0) > 0.39$, was indicative of regular mesopores (Soltani et al., 2014).

The specific surface area and the pore size were calculated using the Brunauer-Emmett-Teller (BET) and Barrett-Joyner-Halenda (BJH) methods, respectively. The textural and structural properties (BET surface area, pore volume, total pore volume, pore diameter, and average pore size) are summarized in Table 6, which also shows that for all of the structural and textural properties studied, sample A2-700 had higher values than the C2-700 sample.

Furthermore, surface area values are larger than those in some studies in the literature for RHA calcined at the same temperature (700 °C). Della et al. (2002) obtained an S_{BET} value of 81 m^2 g^{-1} for ash calcined at 700 °C for 2 h, while Zhang et al. (2015) achieved a value of 136.4 m^2 g^{-1}.

3.2. Quantification of the amorphous silica extracted from the RHAs

Fig. 7 shows the amount and yield of the amorphous silica extracted from agulhinha and cateto RHAs, for different NaOH concentrations and reaction times. According to Fig. 7a, for the concentration of 1 mol L^{-1} of NaOH, the amount of silica extracted increased with reaction time. However, η values for the concentration of 4 mol L^{-1} decreased with the increase in time from 1 to 2 h, but increased significantly with the increase in reaction time to 4 h. Finally, for the concentration of 8 mol L^{-1}, it can be seen that the η values decreased with the increase in time. Therefore, the best results for extraction and yield were obtained in design A-4-4 (concentration of 4 mol L^{-1} of NaOH and reaction time of 4 h).

In Fig. 7b, for the amorphous silica extracted from the cateto RHA, the η value increased with the increase in time from 1 to 2 h, but decreased with the increase in time from 2 to 4 h. However, for the concentration of 4 mol L^{-1}, it can be seen that the η values increased with the increase in reaction time. Finally, for the concentration of 8 mol L^{-1} NaOH, the η values also decreased with the increase in extraction time. Similar to the RHAs obtained from the agulhinha RHs, the best extraction and yield results were obtained in the design using a concentration of 4 mol L^{-1} of NaOH and reaction time of 4 h — the extraction yield value is higher for the RHAs obtained from the agulhinha RHs because the purity of the silica extracted from this variety is about 98.30%.

3.3. Statistical analysis

3.3.1. Analysis of variance and Tukey test

The results obtained in the process for extracting the amorphous silica were submitted to an ANOVA. Table 7 shows the
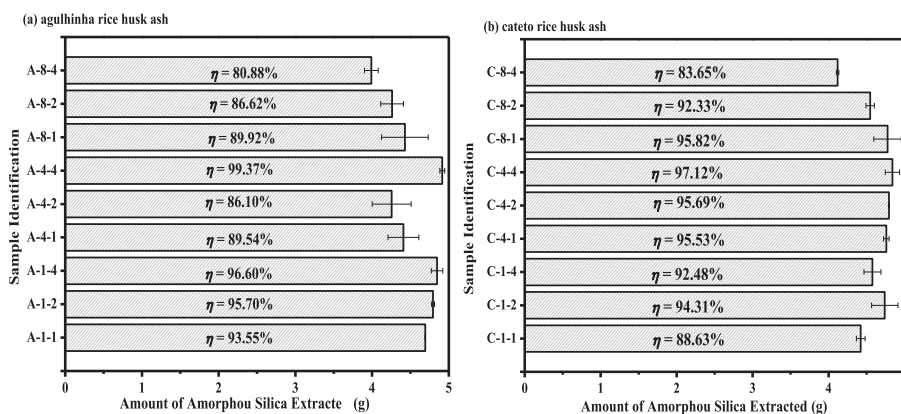
Table 6
Textural and structural properties for the agulhinha and cateto rice husk ash, after 2 h of calcination at 700 °C.

Sample	S_{BET} (m^2 g^{-1})	V (cm^3 g^{-1})	V_T (cm^3 g^{-1})	D_{BJH} (nm)	Average pore size (nm)
A2-700	293.89	0.20	0.36	1.800	2.43
C2-700	173.57	0.10	0.20	1.801	2.32

S_{BET} = BET surface area, V = pore volume, V_T = total pore volume, D_{BJH} = pore diameter.

Fig. 7. Amount of amorphous silica extracted from rice husk ashes (RHAs), as well as yield, using different NaOH concentrations and different reaction times: (a) agulhinha RHAs and (b) cateto RHAs.

Table 7
Analysis of variance parameters for the extraction of silica from the rice husk ashes.

Source of variation	DF	SS	MS	F
Agulhinha rice husk ash				
Treatments	8	1.61	0.20	7.74[a]
Residual	9	0.24	0.03	
Total	17	1.85		
Cateto rice husk ash				
Treatments	8	0.87	0.11	10.61[a]
Residual	9	0.09	0.01	
Total	17	0.96		

[a] Significant at the 5% probability level ($0.01 \leq p < 0.05$), DF = degrees of freedom, SS = sum of squares, MS = mean squared, F = F-statistic value.

ANOVA parameters found for the extraction of silica from the agulhinha and cateto RHAs. It can be seen from Table 7 that there are significant differences in the mean amounts extracted for each treatment — at the 5% significance level, the F-tabulated value with 8 and 9 degrees of freedom is equal to 3.23. Thus, as the F-calculated values were higher than the F-tabulated value, it can be said that at least two of the means are not equal at the 5% significance level.

Although an ANOVA determines whether or not the means of the populations under study are statistically equal, it cannot detect which means are statistically different from the others. Thus, in order to establish the minimum significant difference between the means of the different treatments, the Tukey test had to be applied in order to identify which means are statistically different at 5% probability.

Table 8 shows the results of the Tukey test for the means of the extraction of silica from the agulhinha and cateto RHAs. It can be seen that the means followed by the same letter are not statistically different from each other for the Tukey test at 5% probability. Therefore, it can be seen that the designs that have higher extraction means and no statistical differences are: A-1-1, A-1-2, A-1-4, A-4-1, A-4-4, and A-8-1 (for the agulhinha variety); and C-1-2, C-1-4, C-4-1, C-4-2, C-4-4, C-8-1, and C-8-2 (for the cateto variety). However, the A-4-4 and C-4-4 designs showed higher yields.

4. Conclusions

The chemical composition of the RHs indicated an increase in the percentage of SiO_2 for the RHs treated with HCl, and there was a decrease in the other oxides/impurities with the use of the acid treatment. The acid treatment of the RHs resulted in a small increase in their thermal stability. The XRD profiles showed that the RHs are crystalline; however, the RHAs have amorphous diffraction patterns, due to the presence of amorphous silica. The A2-700 and C2-700 samples had the best calcination parameters and displayed

Table 8
Tukey test for the mean yields of silica extraction from rice husk ashes, using different NaOH concentrations and reaction times.

NaOH (mol L^{-1})	Time (h)		
	1	2	4
Agulhinha rice husk ash			
1	4.6924 ab	4.7945 ab	4.8466 ab
4	4.4083 abc	4.2551 bc	4.9149 a
8	4.4280 abc	4.2602 bc	3.9900 c
Cateto rice husk ash			
1	4.4231 bc	4.7390 ab	4.5773 ab
4	4.7607 ab	4.7791 ab	4.8408 a
8	4.7760 ab	4.5469 ab	4.1190 c

Means followed by the same letter are not statistically different from each other for the Tukey test at 5% probability.

type IV isotherms, with type H1 hysteresis, and good specific surface area values. The best parameters for the extraction of amorphous silica from the RHAs were the A-4-4 and C-4-4 designs, and the extraction yield values varying in the ranges of 80.88–99.37% and 83.65–97.12%, respectively.

Appendix A. Supplementary data

Supplementary data related to this article can be found at https://doi.org/10.1016/j.jclepro.2018.05.028.

References

Adam, F., Iqbal, A., 2010. The oxidation of styrene by chromium-silica heterogeneous catalyst prepared from rice husk. Chem. Eng. J. 160, 742–750. https://doi.org/10.1016/j.cej.2010.04.003.

Adam, F., Kueh, C.W., 2014. Phenyl-amino sulfonic solid acid-MCM-41 complex: a highly active and selective catalyst for the synthesis of mono-alkylated products in the solvent free tert-butylation of phenol. J. Taiwan Inst. Chem. Eng. 45, 713–723. https://doi.org/10.1016/j.jtice.2013.07.008.

An, D., Guo, Y., Zhu, Y., Wang, Z., 2010. A green route to preparation of silica powders with rice husk ash and waste gas. Chem. Eng. J. 162, 509–514. https://doi.org/10.1016/j.cej.2010.05.052.

Artkla, S., Kim, W., Choi, W., Wittayakun, J., 2009. Highly enhanced photocatalytic degradation of tetramethylammonium on the hybrid catalyst of titania and MCM-41 obtained from rice husk silica. Appl. Catal. B Environ. 91, 157–164. https://doi.org/10.1016/j.apcatb.2009.05.019.

Athinarayanan, J., Periasamy, V.S., Alhazmi, M., Alatiah, K.A., Alshatwi, A.A., 2015. Synthesis of biogenic silica nanoparticles from rice husks for biomedical applications. Ceram. Int. 41, 275–281. https://doi.org/10.1016/j.ceramint.2014.08.069.

Bakar, M.S.A., Titiloye, J.O., 2013. Catalytic pyrolysis of rice husk for bio-oil production. J. Anal. Appl. Pyrolysis 103, 362–368. https://doi.org/10.1016/j.jaap.2012.09.005.

Bazargan, A., Bazargan, M., McKay, G., 2015. Optimization of rice husk pretreatment for energy production. Renew. Energy 77, 512–520. https://doi.org/10.1016/j.renene.2014.11.072.

Bhagiyalakshmi, M., Yun, L.J., Anuradha, R., Jang, H.T., 2010. Utilization of rice husk ash as silica source for the synthesis of mesoporous silicas and their application to CO2 adsorption through TREN/TEPA grafting. J. Hazard. Mater. 175, 928–938. https://doi.org/10.1016/j.jhazmat.2009.10.097.

Bledzki, A.K., Mamun, A.A., Volk, J., 2010. Barley husk and coconut shell reinforced polypropylene composites: the effect of fibre physical, chemical and surface properties. Compos. Sci. Technol. 70, 840–846. https://doi.org/10.1016/j.compscitech.2010.01.022.

Carmona, V.B., Oliveira, R.M., Silva, W.T.L., Mattoso, L.H.C., Marconcini, J.M., 2013. Nanosilica from rice husk: extraction and characterization. Ind. Crop. Prod. 43, 291–296. https://doi.org/10.1016/j.indcrop.2012.06.050.

Chauhan, R.P., Kumar, A., 2013. Radon resistant potential of concrete manufactured using Ordinary Portland Cement blended with rice husk ash. Atmos. Environ. 81, 413–420. https://doi.org/10.1016/j.atmosenv.2013.09.024.

Costa, J.A.S., de Jesus, R.A., da Silva, C.M.P., Romão, L.P.C., 2017a. Efficient adsorption of a mixture of polycyclic aromatic hydrocarbons (PAHs) by Si–MCM–41 mesoporous molecular sieve. Powder Technol. 308, 434–441. https://doi.org/10.1016/j.powtec.2016.12.035.

Costa, J.A.S., de Jesus, R.A., Dorst, D.D., Pinatti, I.M., Oliveira, L.M.R., de Mesquita, M.E., Paranhos, C.M., 2017b. Photoluminescent properties of the europium and terbium complexes covalently bonded to functionalized mesoporous material PABA-MCM-41. J. Lumin. 192, 1149–1156. https://doi.org/10.1016/j.jlumin.2017.08.046.

Costa, J.A.S., Garcia, A.C.F.S., Santos, D.O., Sarmento, V.H.V., de Mesquita, M.E., Romão, L.P.C., 2015. Applications of inorganic-organic mesoporous materials constructed by self-assembly processes for removal of benzo[k]fluoranthene and benzo[b]fluoranthene. J. Sol. Gel Sci. Technol. 75, 495–507. https://doi.org/10.1007/s10971-015-3720-6.

Costa, J.A.S., Garcia, A.C.F.S., Santos, D.O., Sarmento, V.H.V., Porto, A.L.M., De Mesquita, M.E., Romão, L.P.C., 2014. A new functionalized MCM-41 mesoporous material for use in environmental applications. J. Braz. Chem. Soc. 25, 197–207. https://doi.org/10.5935/0103-5053.20130284.

Das, A.M., Ali, A.A., Hazarika, M.P., 2014. Synthesis and characterization of cellulose

acetate from rice husk : Eco-friendly condition. Carbohydr. Polym. 112, 342–349. https://doi.org/10.1016/j.carbpol.2014.06.006.

Della, V., Kuhn, I., Hotza, D., 2002. Rice husk ash as an elemente source for active silicaproduction. Mater. Lett. 57, 818–821. https://doi.org/10.1016/S0167-577X(02)00879-0.

Della, V.P., Kühn, I., Hotza, D., 2005. Reciclagem de Resíduos Agro-Industriais : Cinza de Casca de Arroz como Fonte Alternativa de Sílica. Ceram. Ind 10, 22–25.

Della, V.P., Kühn, I., Hotza, D., 2001. Caracterização de Cinza de Casca de Arroz para Uso como Matéria-Prima Na Fabricação de Refratários de Sílica. Quím. Nova 24, 778–782. https://doi.org/10.1017/CBO9781107415324.004.

FAO, 2015. Rice Market Monitor XVI, pp. 1–14.

Ghorbani, F., Younesi, H., Mehraban, Z., elik, M.S., Ghoreyshi, A.A., Anbia, M., 2013. Preparation and characterization of highly pure silica from sedge as agricultural waste and its utilization in the synthesis of mesoporous silica MCM-41. J. Taiwan Inst. Chem. Eng. 44, 821–828. https://doi.org/10.1016/j.jtice.2013.01.019.

Grisdanurak, N., Chiarakorn, S., Wittayakun, J., 2003. Utilization of mesoporous molecular sieves synthesized from natural source rice husk silica to Chlorinated Volatile Organic Compounds (CVOCs) adsorption. Kor. J. Chem. Eng. 20, 950–955. https://doi.org/10.1007/BF02697304.

Gu, S., Zhou, J., Luo, Z., Wang, Q., Ni, M., 2013. A detailed study of the effects of pyrolysis temperature and feedstock particle size on the preparation of nano-silica from rice husk. Ind. Crop. Prod. 50, 540–549. https://doi.org/10.1016/j.indcrop.2013.08.004.

Jang, H.T., Park, Y., Ko, Y.S., Lee, J.Y., Margandan, B., 2009. Highly siliceous MCM-48 from rice husk ash for CO2 adsorption. Int. J. Greenh. Gas Control 3, 545–549. https://doi.org/10.1016/j.ijggc.2009.02.008.

Johar, N., Ahmad, I., Dufresne, A., 2012. Extraction, preparation and characterization of cellulose fibres and nanocrystals from rice husk. Ind. Crop. Prod. 37, 93–99. https://doi.org/10.1016/j.indcrop.2011.12.016.

Kalapathy, U., Proctor, A., Shultz, J., 2002. An improved method for production of silica from rice hull ash. Bioresour. Technol. 85, 285–289. https://doi.org/10.1016/S0960-8524(02)00116-5.

Klemm, D., Heublein, B., Fink, H.P., Bohn, A., 2005. Cellulose: fascinating biopolymer and sustainable raw material. Angew. Chem. Int. Ed. 44, 3358–3393. https://doi.org/10.1002/anie.200460587.

Lee, T., Othman, R., Yeoh, F.Y., 2013. Development of photoluminescent glass derived from rice husk. Biomass Bioenergy 59, 380–392. https://doi.org/10.1016/j.biombioe.2013.08.028.

Muniandy, L., Adam, F., Mohamed, A.R., Ng, E.P., 2014. The synthesis and characterization of high purity mixed microporous/mesoporous activated carbon from rice husk using chemical activation with NaOH and KOH. Microporous Mesoporous Mater. 197, 316–323. https://doi.org/10.1016/j.micromeso.2014.06.020.

Ng, E.P., Awala, H., Tan, K.H., Adam, F., Retoux, R., Mintova, S., 2015. EMT-type zeolite nanocrystals synthesized from rice husk. Microporous Mesoporous Mater. 204, 204–209. https://doi.org/10.1016/j.micromeso.2014.11.017.

Othman Ali, I., Hassan, A.M., Shaaban, S.M., Soliman, K.S., 2011. Synthesis and characterization of ZSM-5 zeolite from rice husk ash and their adsorption of Pb2+ onto unmodified and surfactant-modified zeolite. Sep. Purif. Technol. 83, 38–44. https://doi.org/10.1016/j.seppur.2011.08.034.

Qiu, K.-Z., Guo, W.-W., Wang, H.-X., Zhu, L.-J., Wang, S.-R., 2015. Influence of catalyst structure on performance of Cu/SiO2 in hydrogenation of methyl acetate. Acta Physico-Chim. Sin. 31, 1129–1136. https://doi.org/10.3866/PKU.WHXB201503272.

Raabe, J., De Souza Fonseca, A., Bufalino, L., Ribeiro, C., Martins, M.A., Marconcini, J.M., Tonoli, G.H.D., 2014. Evaluation of reaction factors for deposition of silica (SiO2) nanoparticles on cellulose fibers. Carbohydr. Polym. 114, 424–431. https://doi.org/10.1016/j.carbpol.2014.08.042.

Rambo, M.K.D., Cardoso, A.L., Bevilaqua, D.B., Rizzetti, T.M., Ramos, L.A., Korndörfer, G.H., Martins, A.F., 2011. Silica from rice Husk Ash as an additive for rice plant. J. Agron. 10, 99–104. https://doi.org/10.3923/ja.2011.99.104.

Real, C., Alcala, M.D., Criado, J.M., 1996. Preparation of silica from rice husks. J. Am. Ceram. Soc. 79, 2012–2016. https://doi.org/10.1111/j.1151-2916.1996.tb08931.x.

Santos, D.O., Santos, M.L.N., Costa, J.A.S., de Jesus, R.A., Navickiene, S., Sussuchi, E.M., de Mesquita, M.E., 2013. Investigating the potential of functionalized MCM-41 on adsorption of Remazol Red dye. Environ. Sci. Pollut. Res. 20, 5028–5035. https://doi.org/10.1007/s11356-012-1346-6.

Seliem, M.K., Komarneni, S., Parette, R., Katsuki, H., Cannon, F.S., Shahien, M.G., Khalil, A.A., El-Gaid, I.M.A., 2011. Perchlorate uptake by organosilicas, organo-clay minerals and composites of rice husk with MCM-48. Appl. Clay Sci. 53, 621–626. https://doi.org/10.1016/j.clay.2011.05.012.

Silva, F. de A.S. e, Azevedo, C.A.V. de, 2002. Versão do programa computacional Assistat para o sistema operacional Windows. Rev. Bras. Prod. Agroind. 4, 71–78. https://doi.org/10.1517-8595.

Soares, L.W.O., Braga, R.M., Freitas, J.C.O., Ventura, R.A., Pereira, D.S.S., Melo, D.M.A., 2015. The effect of rice husk ash as pozzolan in addition to cement Portland class G for oil well cementing. J. Petrol. Sci. Eng. 131, 80–85. https://doi.org/10.1016/j.petrol.2015.04.009.

Soltani, N., Bahrami, A., González, L.A., 2014. Review on the physicochemical treatments of rice husk for productionof advanced materials. Chem. Eng. J. 264, 899–935. https://doi.org/10.1016/j.cej.2014.11.056.

Tran, T.P.T., Bénézet, J.C., Bergeret, A., 2014. Rice and Einkorn wheat husks reinforced poly(lactic acid) (PLA) biocomposites: effects of alkaline and silane surface treatments of husks. Ind. Crop. Prod. 58, 111–124. https://doi.org/10.1016/j.indcrop.2014.04.012.

Wang, S., Guo, W.-W., Wang, H.-X., Zhu, L., Luo, Z., 2011. Highly active and selective Cu/SiO2 catalysts prepared by the urea hydrolysis method in dimethyl oxalate hydrogenation. Catal. Commun. 12, 1246–1250. https://doi.org/10.1016/j.catcom.2011.04.019.

Wantala, K., Khongkasem, E., Khlongkarnpanich, N., Sthiannopkao, S., Kim, K.W., 2012. Optimization of As(V) adsorption on Fe-RH-MCM-41-immobilized GAC using Box-Behnken Design: effects of pH, loadings, and initial concentrations. Appl. Geochem. 27, 1027–1034. https://doi.org/10.1016/j.apgeochem.2011.11.014.

Yeh, S.K., Hsieh, C.C., Chang, H.C., Yen, C.C.C., Chang, Y.C., 2015. Synergistic effect of coupling agents and fiber treatments on mechanical properties and moisture absorption of polypropylene-rice husk composites and their foam. Compos. Part A Appl. Sci. Manuf 68, 313–322. https://doi.org/10.1016/j.compositesa.2014.10.019.

Yeletsky, P.M., Yakovlev, V.A., Mel'gunov, M.S., Parmon, V.N., 2009. Synthesis of mesoporous carbons by leaching out natural silica templates of rice husk. Microporous Mesoporous Mater. 121, 34–40. https://doi.org/10.1016/j.micromeso.2008.12.025.

Zhang, H., Ding, X., Chen, X., Ma, Y., Wang, Z., Zhao, X., 2015. A new method of utilizing rice husk: consecutively preparing d-xylose, organosolv lignin, ethanol and amorphous superfine silica. J. Hazard. Mater. 291, 65–73. https://doi.org/10.1016/j.jhazmat.2015.03.003.

Zhang, M.-H., Malhotra, V.M., 1996. High-performance concrete incorporating rice husk ash as a supplementary cementing material. ACI Mater. J. 93, 629–636.